Supporting Information for "Morphodynamics of barchan-barchan interactions investigated at the grain scale"

An edited version of this paper was published by AGU. Copyright (2021) American Geophysical Union. Assis, W. R. and Franklin, E. M. (2021). Morphodynamics of barchan-barchan interactions investigated at the grain scale. Journal of Geophysical Research: Earth Surface, 126, e2021JF006237. https://doi.org/10.1029/2021JF006237.

To view the published open abstract, go to https://doi.org/10.1029/2021JF006237.

W. R. Assis[1], E. M. Franklin[1]

[1]School of Mechanical Engineering, UNICAMP - University of Campinas,

Rua Mendeleyev, 200, Campinas, SP, Brazil

Contents of this file

1. Figures S1 to S19
2. Tables S1 and S2

Additional Supporting Information (Files uploaded separately)

1. Captions for Movies S1 to S22

Introduction

This supporting information presents microscopy images of the used grains, additional graphics, lists of the tested conditions, and movies showing examples of grains'

displacements for each interaction pattern. We note that the images that were processed to plot the figures shown in the paper are available on Mendeley Data (http://dx.doi.org/10.17632/f9p59sxm4f).

The experimental device is the same as in Assis and Franklin (2020), and is described in the paper. We describe briefly in this supporting information the PIV (particle image velocimetry) experiments that were performed in the test section of the channel in the absence of grains in order to determine the shear velocity of the base flow u_*. Our tests were performed with a two-dimensional two-component particle image velocimetry (2D2C-PIV) device, where a laser sheet was positioned in the vertical plane of symmetry of the channel, and a camera of CCD type (charge-coupled device) was placed perpendicularly to the laser sheet. We used a dual-cavity Nd:YAG Q-switched laser emitting up to 2 $\times$ 130 mJ at a maximum pulse rate of 15 Hz, and a 2048 px $\times$ 2048 px camera with a CCD sensor measuring 7.4 μm $\times$ 7.4 μm (px^2). Once the camera and laser were synchronized, the maximum acquisition rate of image pairs was 4 Hz, and the time between frames was adjusted in accordance with the flow velocity. We used hollow glass spheres with mean diameter of 10 μm and S.G. = 1.05 as seeding particles, and the magnification was approximately 0.1. After focusing the camera on the laser plane, adjusting the inter-frame time and calibrating the image (from px to mm), we imposed different water flow rates (mono-phase flows) and acquired the PIV images.

From image processing, we obtained profiles whose mean averages followed closely the law of the wall, $u^+ = 1/\kappa \ln y^+ + B$, where u^+ is the mean velocity normalized by u_*, $\kappa = 0.41$ is the von Kármán constant, $y^+ = y\nu/u_*$ is the vertical coordinate normalized by the viscous length, ν is the kinematic viscosity and B is a constant. The experimental values

of u_* and Darcy friction factor $f = 8(u_*)^2(U)^{-2}$, where U is the cross-sectional mean velocity, were then obtained from the inclination of $u^+(y^+)$. The experimental values of f were compared with the Darcy friction factor computed from the Blasius correlation, $f_{bla} = 0.316Re_{dh}^{-1/4}$, where $Re_{dh} = Ud_h/\nu$ and $d_h = 3.05\ \delta$ is the hydraulic diameter (cross-sectional area multiplied by four and divided by the cross-sectional perimeter, δ being the channel half height). The differences between experimental and correlated friction factors were equal or less than 6 %, implying differences in u_* of less than 3 %.

Movie S1. Chasing_Aligned_t1.gif Movie showing a sequence of 10 images of the chasing pattern in aligned configuration during a first stage of interaction. It is possible to follow the moving grains in the movie.

Movie S2. Chasing_Aligned_t2.gif Movie showing a sequence of 10 images of the chasing pattern in aligned configuration during a second stage of interaction. It is possible to follow the moving grains in the movie.

Movie S3. Chasing_OffCentered_t1.gif Movie showing a sequence of 10 images of the chasing pattern in off-centered configuration during a first stage of interaction. It is possible to follow the moving grains in the movie.

Movie S4. Chasing_OffCentered_t2.gif Movie showing a sequence of 10 images of the chasing pattern in off-centered configuration during a second stage of interaction. It is possible to follow the moving grains in the movie.

Movie S5. Merging_Aligned_t1.gif Movie showing a sequence of 10 images of the merging pattern in aligned configuration during a first stage of interaction. It is possible to follow the moving grains in the movie.

Movie S6. Merging_Aligned_t2.gif Movie showing a sequence of 10 images of the merging pattern in aligned configuration during a second stage of interaction. It is possible to follow the moving grains in the movie.

Movie S7. Merging_OffCentered_t1.gif Movie showing a sequence of 10 images of the merging pattern in off-centered configuration during a first stage of interaction. It is possible to follow the moving grains in the movie.

Movie S8. Merging_OffCentered_t2.gif Movie showing a sequence of 10 images of the merging pattern in off-centered configuration during a second stage of interaction. It is possible to follow the moving grains in the movie.

Movie S9. Exchange_Aligned_t1.gif Movie showing a sequence of 10 images of the exchange pattern in aligned configuration during a first stage of interaction. It is possible to follow the moving grains in the movie.

Movie S10. Exchange_Aligned_t2.gif Movie showing a sequence of 10 images of the exchange pattern in aligned configuration during a second stage of interaction. It is possible to follow the moving grains in the movie.

Movie S11. Exchange_OffCentered_t1.gif Movie showing a sequence of 10 images of the exchange pattern in off-centered configuration during a first stage of interaction. It is possible to follow the moving grains in the movie.

Movie S12. Exchange_OffCentered_t2.gif Movie showing a sequence of 10 images of the exchange pattern in off-centered configuration during a second stage of interaction. It is possible to follow the moving grains in the movie.

Movie S13. FragChasing_Aligned_t1.gif Movie showing a sequence of 10 images of the fragmentation-chasing pattern in aligned configuration during a first stage of interaction. It is possible to follow the moving grains in the movie.

Movie S14. FragChasing_Aligned_t2.gif Movie showing a sequence of 10 images of the fragmentation-chasing pattern in aligned configuration during a second stage of interaction. It is possible to follow the moving grains in the movie.

Movie S15. FragChasing_Aligned_t3.gif Movie showing a sequence of 10 images of the fragmentation-chasing pattern in aligned configuration during a third stage of interaction. It is possible to follow the moving grains in the movie.

Movie S16. FragChasing_OffCentered_t1.gif Movie showing a sequence of 10 images of the fragmentation-chasing pattern in off-centered configuration during a first stage of interaction. It is possible to follow the moving grains in the movie.

Movie S17. FragChasing_OffCentered_t2.gif Movie showing a sequence of 10 images of the fragmentation-chasing pattern in off-centered configuration during a second stage of interaction. It is possible to follow the moving grains in the movie.

Movie S18. FragChasing_OffCentered_t3.gif Movie showing a sequence of 10 images of the fragmentation-chasing pattern in off-centered configuration during a third stage of interaction. It is possible to follow the moving grains in the movie.

Movie S19. FragExchange_Aligned_t1.gif Movie showing a sequence of 10 images of the fragmentation-exchange pattern in aligned configuration during a first stage of interaction. It is possible to follow the moving grains in the movie.

Movie S20. FragExchange_Aligned_t2.gif Movie showing a sequence of 10 images of the fragmentation-exchange pattern in aligned configuration during a second stage of interaction. It is possible to follow the moving grains in the movie.

Movie S21. FragExchange_OffCentered_t1.gif Movie showing a sequence of 10 images of the fragmentation-exchange pattern in off-centered configuration during a first stage of interaction. It is possible to follow the moving grains in the movie.

Movie S22. FragExchange_OffCentered_t2.gif Movie showing a sequence of 10 images of the fragmentation-exchange pattern in off-centered configuration during a second stage of interaction. It is possible to follow the moving grains in the movie.

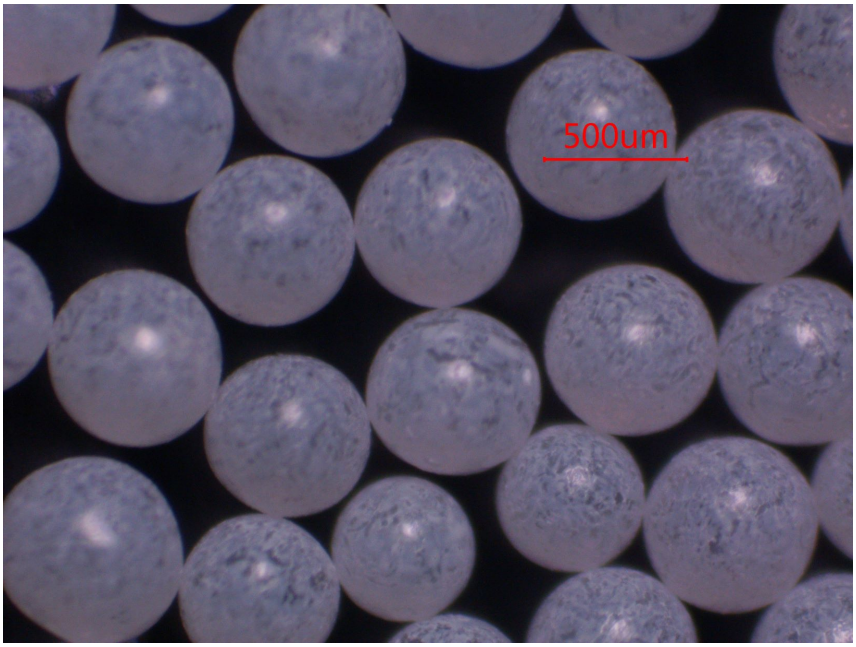

Figure S1. Microscopy image for the 0.40 mm $\leq d \leq$ 0.60 mm round glass beads of white color.

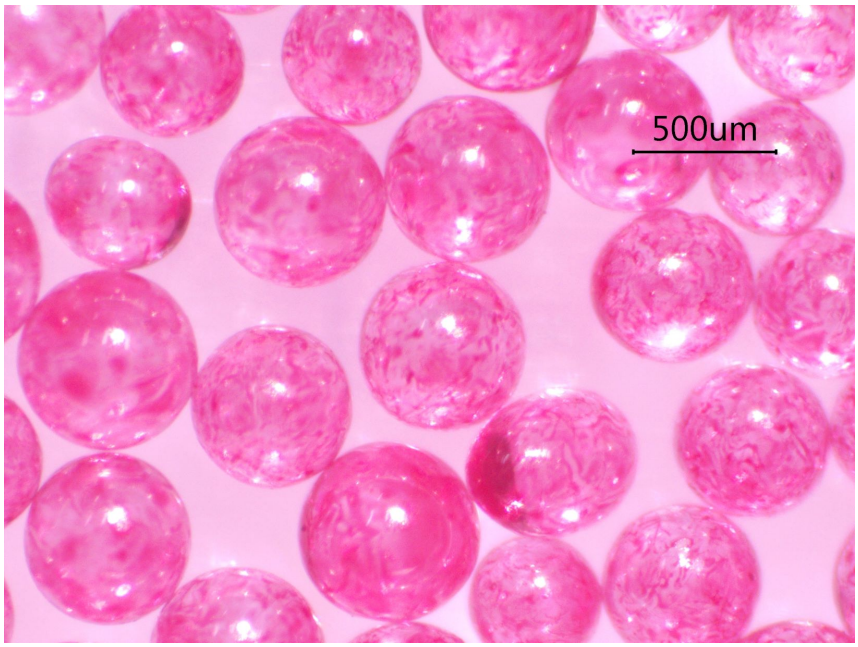

Figure S2. Microscopy image for the 0.40 mm $\leq d \leq$ 0.60 mm round glass beads of red color.

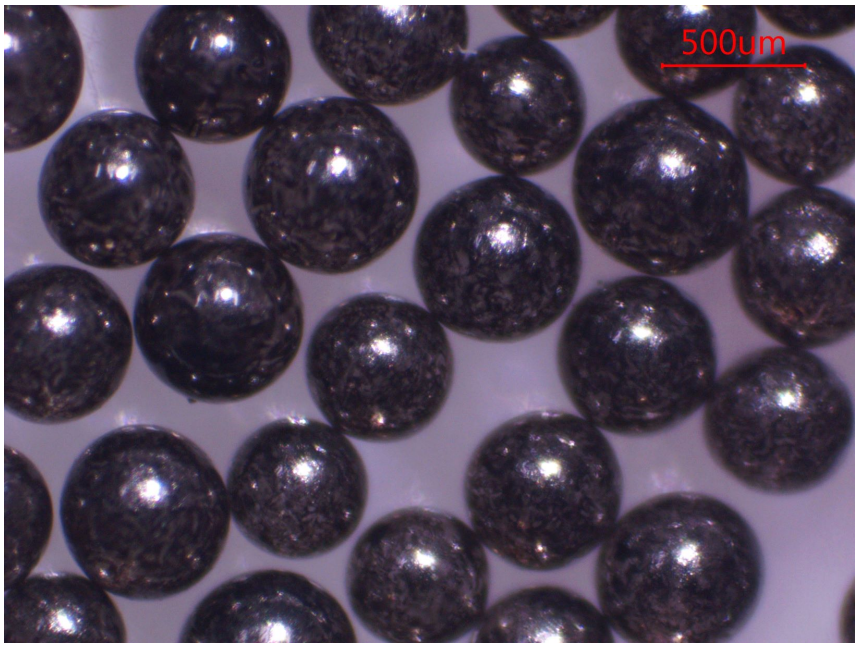

Figure S3. Microscopy image for the 0.40 mm $\leq d \leq$ 0.60 mm round glass beads of black color.

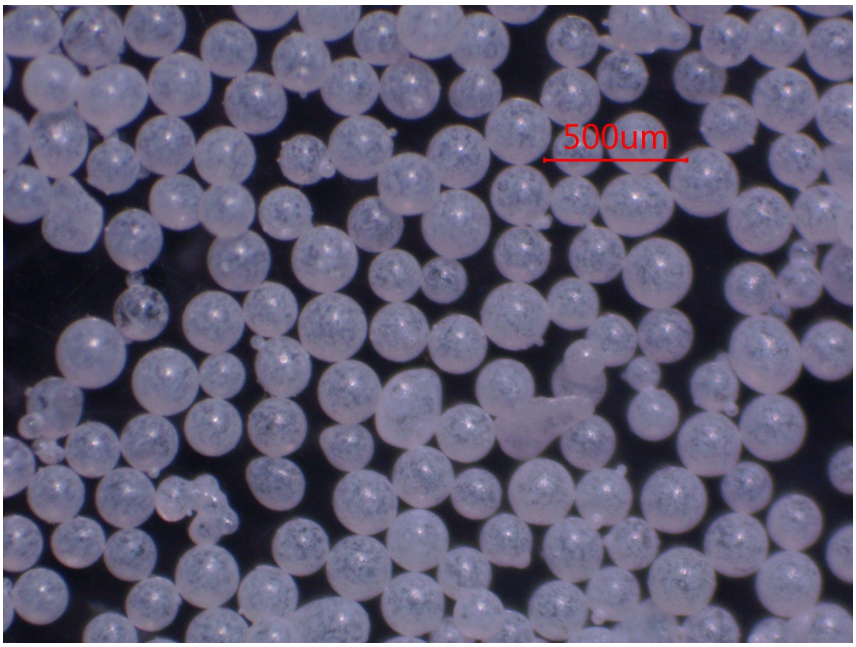

Figure S4. Microscopy image for the 0.15 mm $\leq d \leq$ 0.25 mm round glass beads of white color.

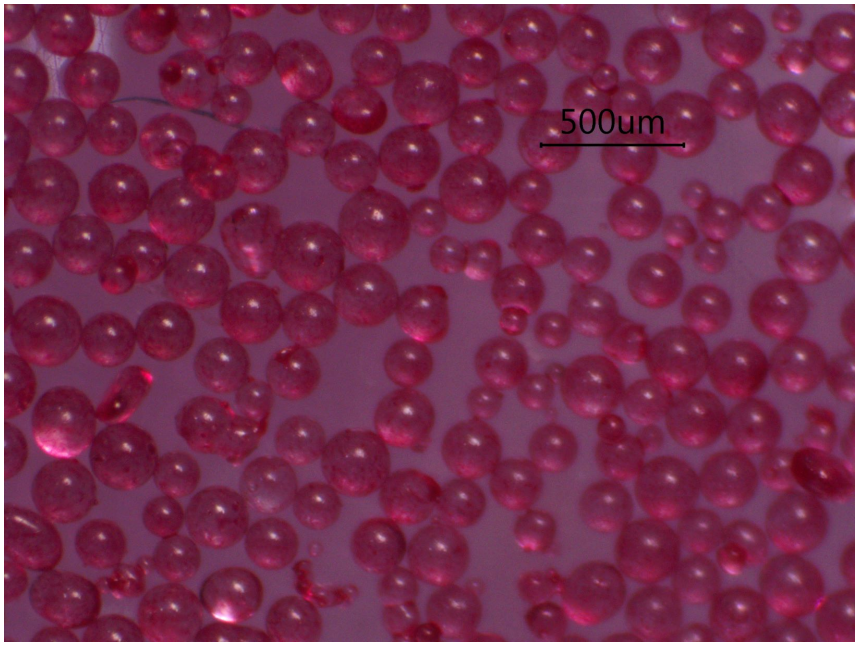

Figure S5. Microscopy image for the 0.15 mm $\leq d \leq$ 0.25 mm round glass beads of red color.

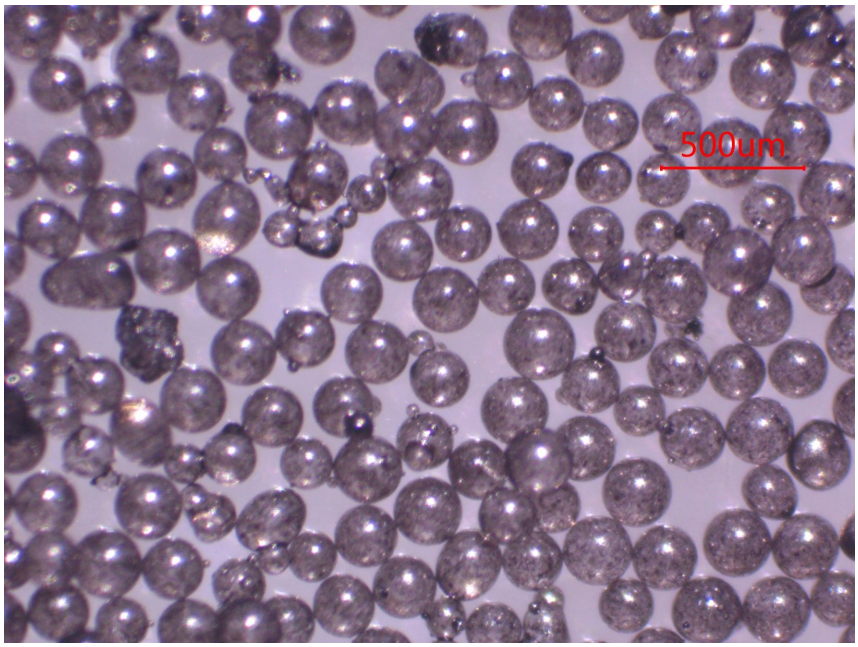

Figure S6. Microscopy image for the 0.15 mm $\leq d \leq$ 0.25 mm round glass beads of black color.

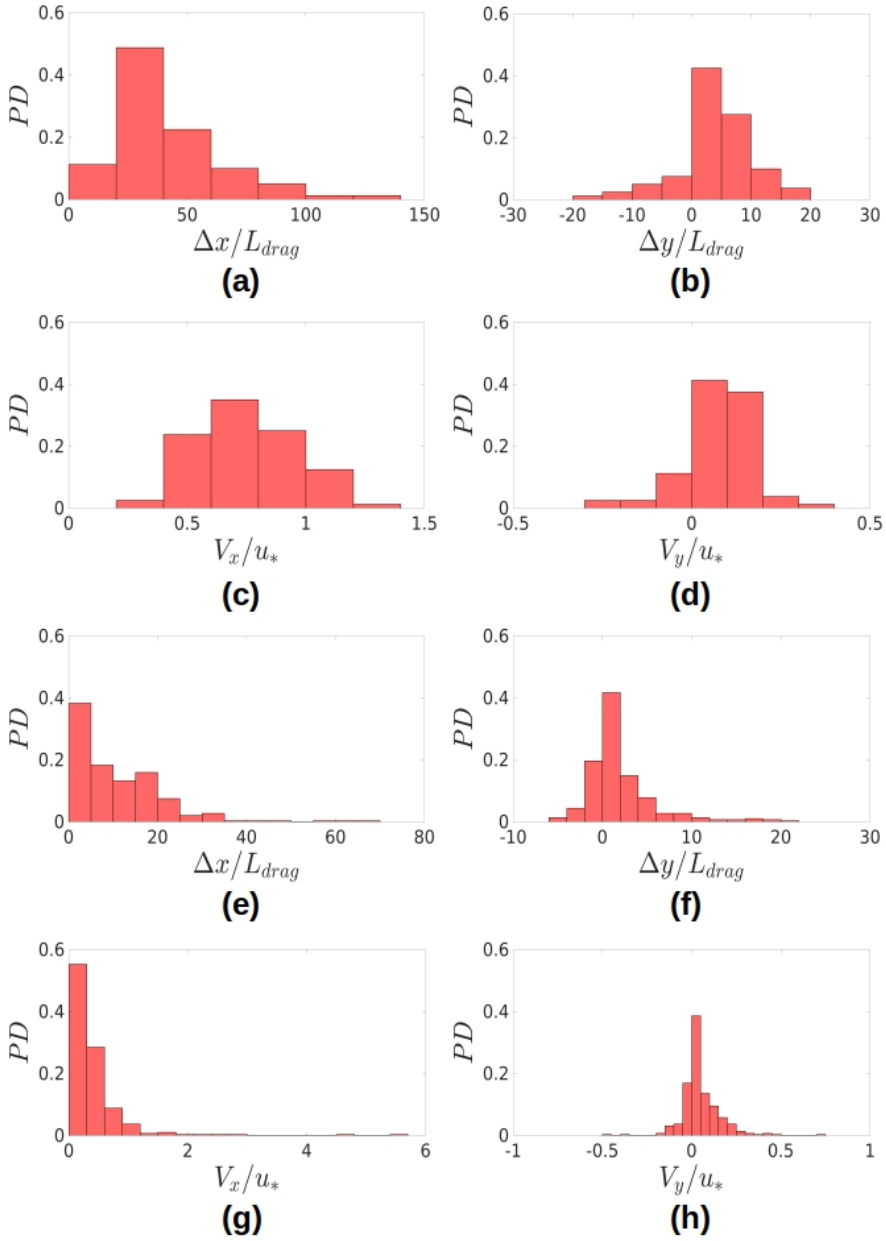

Figure S7. Probability distributions (PDs), for grains exchanged between barchans, of total distances traveled by grains, Δx and Δy, and time-averaged velocities, V_x and V_y. Figures (a) to (d) correspond to the chasing pattern (red trajectories in Figure 2d of the paper) and Figures (e) to (h) to the merging pattern (red trajectories in Figure 3b of the paper).

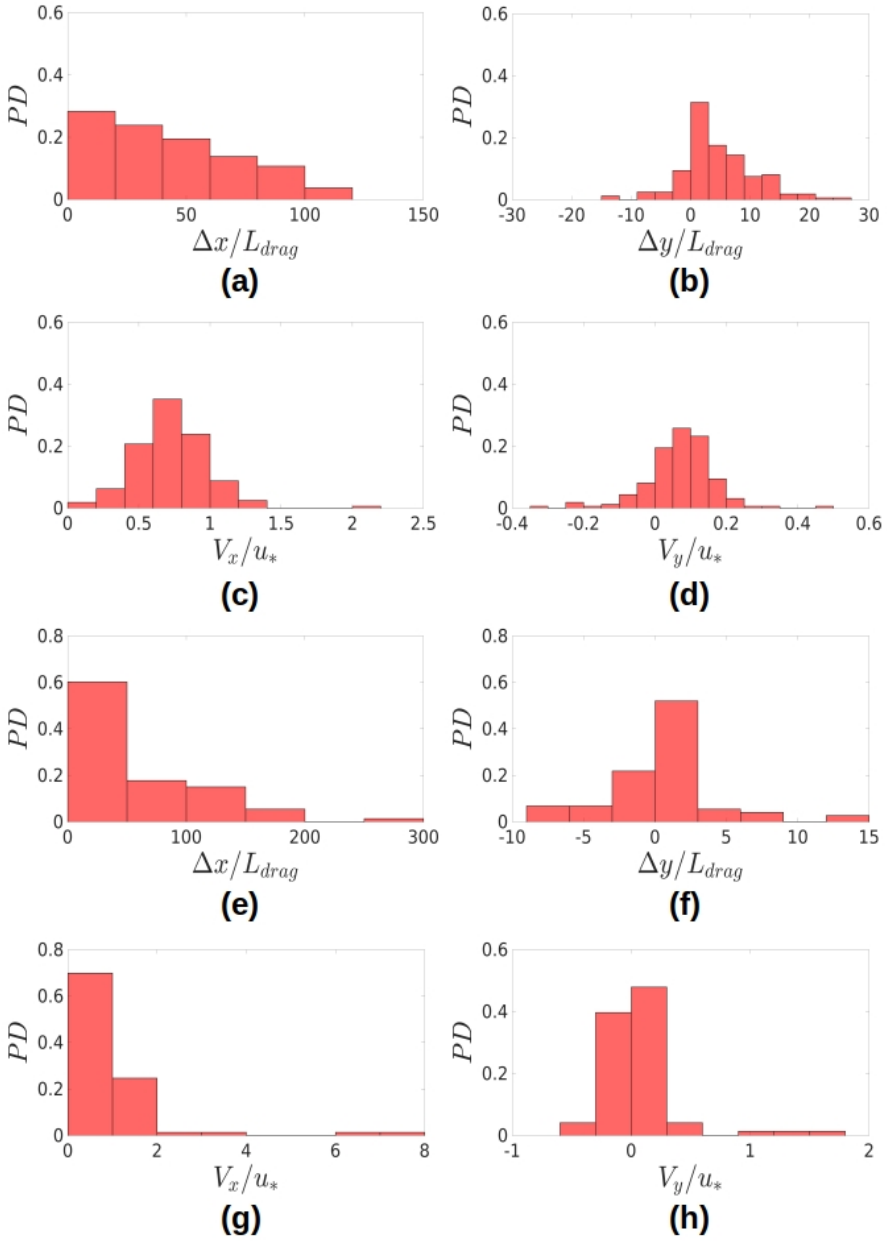

Figure S8. Probability distributions (PDs), for grains exchanged between barchans, of total distances traveled by grains, Δx and Δy, and time-averaged velocities, V_x and V_y. All figures concern the fragmentation-chasing pattern, Figures (a) to (d) corresponding to the red trajectories in Figure 5a of the paper and Figures (e) to (h) to the red trajectories in Figure 5f of the paper.

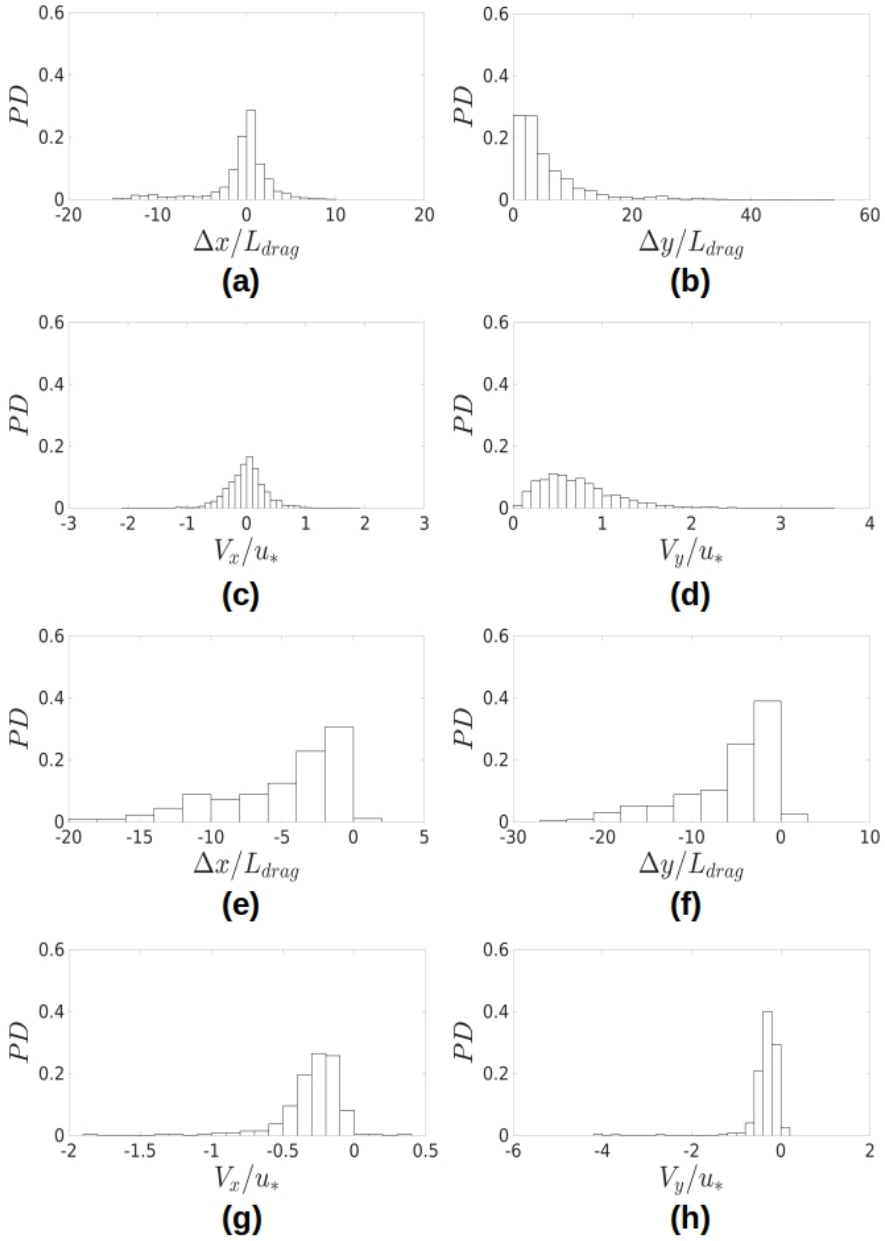

Figure S9. Probability distributions (PDs), for grains exchanged between barchans, of total distances traveled by grains, Δx and Δy, and time-averaged velocities, V_x and V_y. Figures (a) to (d) correspond to the fragmentation-exchange pattern (white trajectories in Figure 6c of the paper) and Figures (e) to (h) to the exchange pattern (white trajectories in Figure 4d of the paper).

Figure	N	Δt (s)	Figure	N	Δt (s)	Figure	N	Δt (s)
7a	226	15	s7a	80	15	s9a	1326	7.5
7b	226	15	s7b	80	15	s9b	1326	7.5
7c	317	15	s7c	80	15	s9c	1326	7.5
7d	317	15	s7d	80	15	s9d	1326	7.5
7e	107	7.5	s7e	295	15	s9e	272	5
7f	95	7.5	s7f	295	15	s9f	272	5
7g	112	7.5	s7g	295	15	s9g	272	5
7h	112	7.5	s7h	295	15	s9h	272	5
8a	243	5	s8a	159	7.5			
8b	243	5	s8b	159	7.5			
8c	243	5	s8c	159	7.5			
8d	243	5	s8d	159	7.5			
8e	48	7.5	s8e	73	7.5			
8f	48	7.5	s8f	73	7.5			
8g	48	7.5	s8g	73	7.5			
8h	48	7.5	s8h	73	7.5			

Figure S10. Number of grains N followed during Δt to plot the probability distributions shown in Figures 7 and 8 of the paper and S7, S8 and S9 of the supporting information. The columns *Figure* correspond to the respective subfigures.

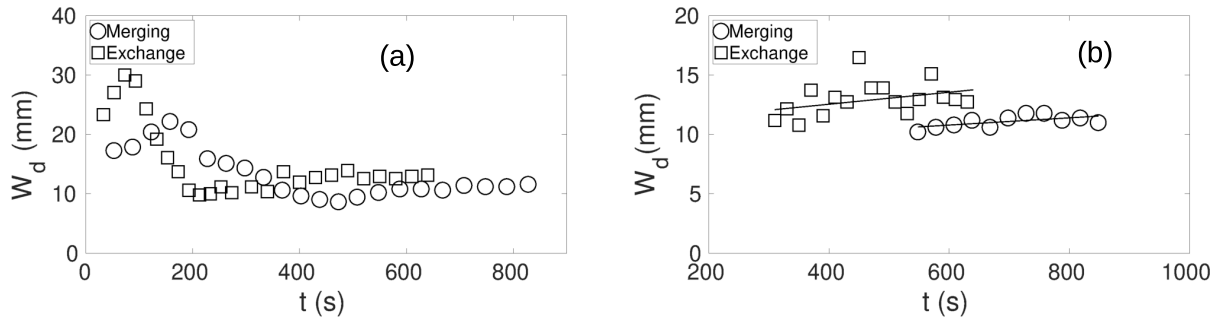

Figure S11. Width of the longitudinal stripe W_d as a function of time during (a) the entire collision processes; (b) the second stage of merging and exchange interactions. Circles and squares correspond to merging and exchange interactions, respectively, and continuous lines are linear fittings.

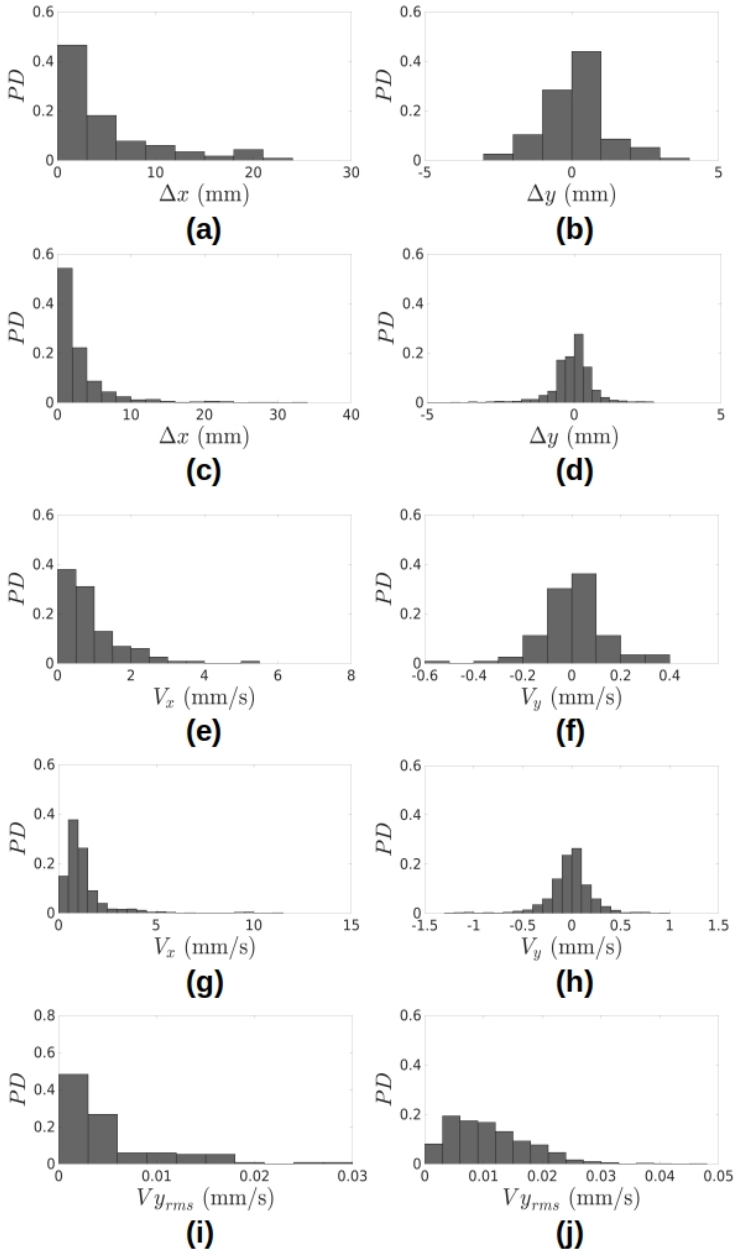

Figure S12. Probability distributions (PDs), for grains from the impact barchan spreading over the target one, of total distances traveled by grains, Δx and Δy, time-averaged velocities, V_x and V_y, and RMS averages of the transverse velocity of each grain Vy_{rms}, in dimensional form. Figures (a),(b),(e),(f) and (i) correspond to the merging pattern and Figures (c),(d),(g),(h) e (j) to the exchange pattern.

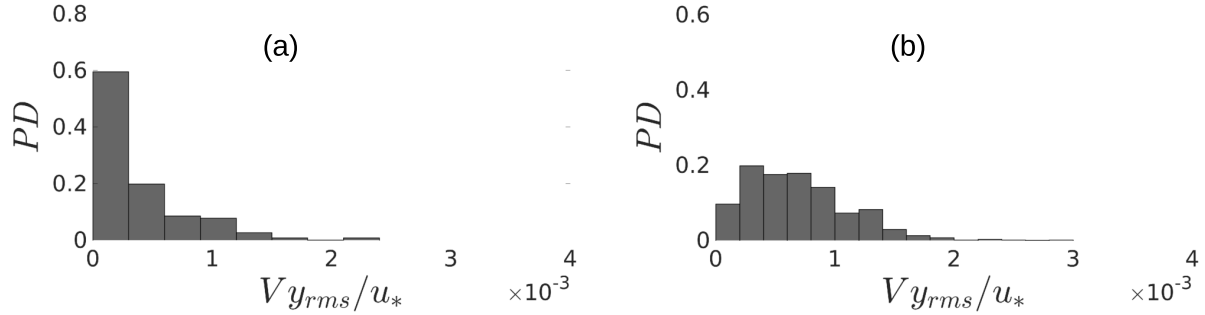

Figure S13. PDs of the RMS average of the transverse velocity of each grain. Figure (a) corresponds to the merging and Figure (b) to the exchange pattern.

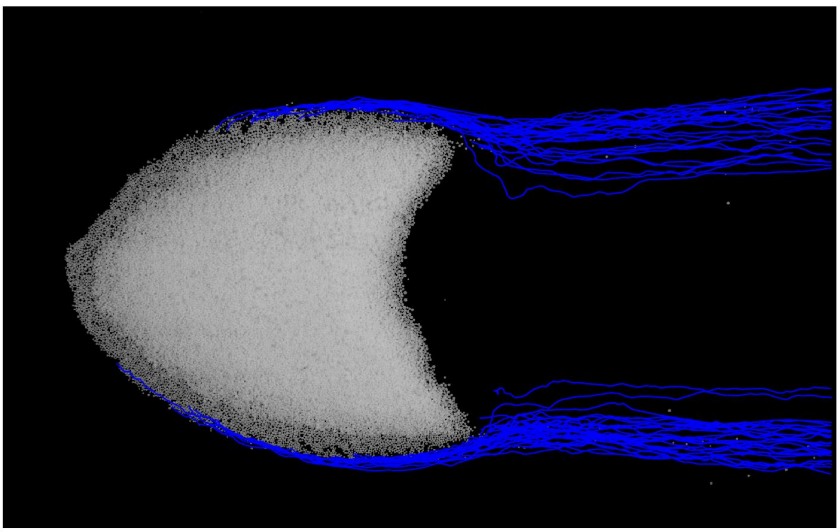

Figure S14. Trajectories of some grains leaving an isolated barchan dune. The barchan was formed from a 10 g pile consisting of $d = 0.5$ mm glass beads, and the imposed water flow had $u_* = 0.0159$ m/s.

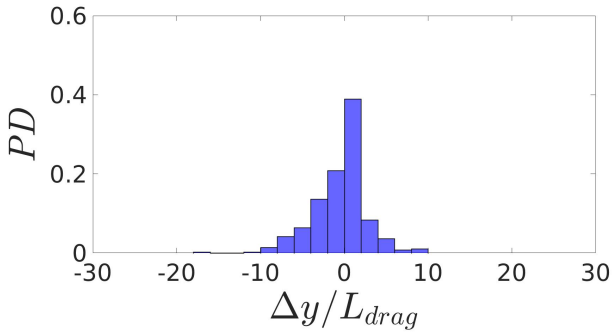

Figure S15. Probability distribution (PD) of total distances traveled by grains in the transverse direction Δy for grains leaving an isolated barchan (some of the trajectories are shown in Figure S14), normalized by L_{drag}. Mean value and standard deviation are -0.62 and 3.16, respectively. This PD corresponds to a duration of 10 s, where 359 grains were tracked.

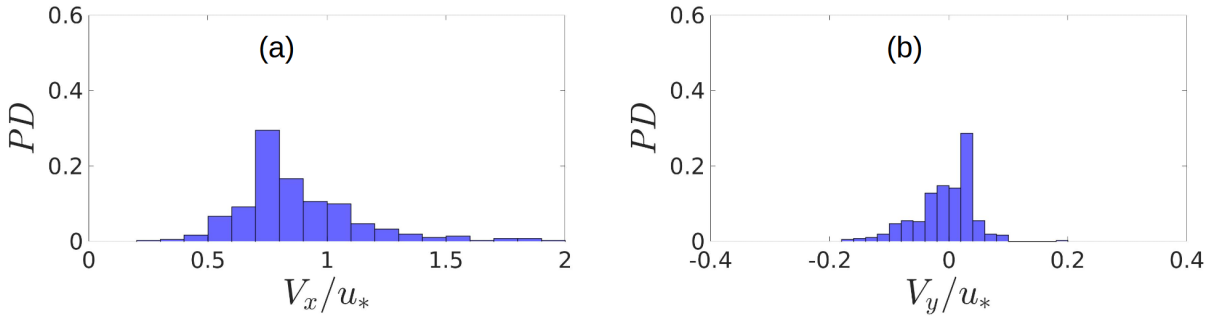

Figure S16. Probability distributions (PDs) of time-averaged velocities (a) V_x and (b) V_y for grains leaving an isolated barchan (some of the trajectories are shown in Figure S14), normalized by u_*. Mean values are $V_x/u_* = 0.88$ and $V_y/u_* =$ -0.006, with the respective standard deviations 0.25 and 0.048. These PDs correspond to a duration of 10 s, where 359 grains were tracked.

Chasing									
Figure paper	Followed (red trajectories)	Total number followed	% followed	Total moving particles	Time interval (s)	Going over downstream barchan	Going around downstream barchan	Directly entrained downstream	Flux difference
2b	310	844	96%	879	7.5	24%	7%	69%	18%
2d	111	351	96%	366	15	28%	44%	28%	33%
Merging									
Figure paper	Followed (red trajectories)	Total number followed	% followed	Total moving particles	Time interval (s)	Going over downstream barchan + going around downstream barchan			
3a	235	353	96%	368	15	92%			
3c	143	321	96%	334	15	1%			
Exchange									
Figure paper	Followed (white trajectories)	Total number followed	% followed	Total moving particles	Time interval (s)	Migrating from the new ejected barchan (baby barchan) toward the upstream bedform			
4b	243	2129	96%	2218	5	22%			
Frag-Chasing									
Figure paper	Followed (red trajectories)	Total number followed	% followed	Total moving particles	Time interval (s)	Flux difference			
5a	159	377	98%	385	7.5	73%			
5d	34	195	98%	199	5	19%			
Frag-Exchange									
Figure paper	Followed (white trajectories)	Total number followed	% followed	Total moving particles	Time interval (s)	Grains entrained from the downstream bedform toward the impact barchan			
6a	48	100	98%	102	7.5	46%			
6b	30	72	98%	73	7.5	42%			
6c	1326	1699	98%	1734	7.5	70%			
6d	67	1132	98%	1155	7.5	5%			

Figure S17. Percentages of grains exchanged between dunes for some cases presented in the paper. The first six columns correspond to figure numbers in the paper, number of followed grains for the indicated trajectories, total number of followed grains, percentages of followed grains (of the total), total number of moving grains (estimated from percentages), and time interval in which those particles were followed.

Chasing									
Figure paper	Followed (red trajectories)	Total number followed	% followed	Total moving particles	Time interval (s)	M going over downstream barchan (g/s)	M going around downstream barchan (g/s)	M directly entrained downstream (g/s)	ΔM (g/s)
2b	310	844	96%	879	7.5	4.60E-03	1.34E-03	1.32E-02	3.45E-03
2d	111	351	96%	366	15	1.12E-03	1.75E-03	1.12E-03	1.32E-03
Merging									
Figure paper	Followed (red trajectories)	Total number followed	% followed	Total moving particles	Time interval (s)	M going over downstream barchan + going around downstream barchan (g/s)			
3a	235	353	96%	368	15	3.69E-03			
3c	143	321	96%	334	15	3.65E-05			
Exchange									
Figure paper	Followed (white trajectories)	Total number followed	% followed	Total moving particles	Time interval (s)	M migrating from the new ejected barchan (baby barchan) toward the upstream bedform (g/s)			
4b	243	2129	96%	2218	5	1.02E-03			
Frag-Chasing									
Figure paper	Followed (red trajectories)	Total number followed	% followed	Total moving particles	Time interval (s)	ΔM (g/s)			
5a	159	377	98%	385	7.5	3.92E-04			
5d	34	195	98%	199	5	7.92E-05			
Frag-Exchange									
Figure paper	Followed (white trajectories)	Total number followed	% followed	Total moving particles	Time interval (s)	M grains entrained from the downstream bedform toward the impact barchan (g/s)			
6a	48	100	98%	102	7.5	6.55E-05			
6b	30	72	98%	73	7.5	4.31E-05			
6c	1326	1699	98%	1734	7.5	1.69E-03			
6d	67	1132	98%	1155	7.5	8.06E-05			

Figure S18. Mass flow rates M (in g/s) of grains exchanged between dunes for some cases presented in the paper. ΔM is the net mass flow rate, and the first six columns are the same as in Figure S17.

Pattern	Chasing			Merging				Exchange		
Figure (paper)	2a	2b	2d	3a	3b	3c	3d	4b	4d	
mean V_x / u·	1.31	1.13	0.75	0.71	0.41	1.33	0.62	0.55	-0.29	
Standard deviation V_x/u·	0.54	0.34	0.22	0.37	0.54	0.03	0.46	0.31	0.22	
mean V_y/u·	-0.01	0.23	0.07	0.06	0.05	0.18	0.04	0.37	-0.34	
Standard deviationV_y/u·	0.16	0.10	0.10	0.14	0.11	0.02	0.10	1.13	0.40	
Mean $\Delta x/L_{drag}$	55.18	34.45	40.74	33.39	10.80	107.20	12.56	9.11	-5.06	
Standard deviation $\Delta x/L_{drag}$	28.32	14.27	23.55	18.16	10.30	3.84	12.70	5.35	4.27	
Mean $\Delta y/L_{drag}$	-0.11	6.90	3.75	2.44	1.96	-15.16	1.25	8.01	-5.76	
Standard deviation $\Delta y/L_{drag}$	5.96	3.70	6.35	6.65	3.92	2.98	2.37	17.83	5.35	
Pattern	Frag-chasing						Frag-exchange			
Figure (paper)	5a	5b	5c	5d	5e	5f	6a	6b	6c	6d
mean V_x / u·	0.73	1.01	1.01	2.63	1.21	1.01	-0.10	-0.17	0.00	-0.32
Standard deviation V_x/u·	0.26	0.45	0.39	2.31	0.30	1.12	0.06	0.08	0.33	0.13
mean V_y/u·	0.07	-0.01	-0.08	-0.14	0.03	0.07	-0.14	-0.36	0.72	0.19
Standard deviationV_y/u·	0.10	0.21	0.19	0.86	0.10	0.31	0.18	0.16	0.43	0.17
Mean $\Delta x/L_{drag}$	41.79	47.30	35.31	46.11	130.43	47.85	-7.16	-8.80	-0.66	-7.35
Standard deviation $\Delta x/L_{drag}$	30.41	30.69	28.92	41.32	54.05	59.51	3.51	2.81	3.51	3.75
Mean $\Delta y/L_{drag}$	4.58	-2.71	-2.81	-4.06	2.66	0.13	-6.26	-20.18	5.50	3.99
Standard deviation $\Delta y/L_{drag}$	6.18	10.62	7.65	5.80	8.36	3.75	11.36	8.77	6.02	2.85

Figure S19. Mean values and standard deviations of Δx, Δy, V_x and V_y for the trajectories indicated in the line *Figure (paper)*, which lists the corresponding figure numbers in the paper. The colors of the cells are the same as those of trajectories in the corresponding figure.

Table S1. List of the tested conditions in the aligned configuration. σ is the offset parameter, m_i and m_t are the masses of the impacting (upstream) and target (downstream) dunes, respectively, N_i and N_t are the numbers of grains of the impacting and target dunes, respectively, ξ_N is the dimensionless particle number, ρ_s and d are the density and mean diameter of grains, respectively, u_* is the shear velocity, Re_* is the particle Reynolds number, θ is the Shields number, and *Pattern* corresponds to the collision pattern. For definitions of σ and ξ_N, please refer to Assis and Franklin, Geophys. Res. Lett., 47, e2020GL089464, 2020, https://doi.org/10.1029/2020GL089464.

σ	m_i	m_t	N_i	N_t	ξ_N	ρ_s	d	u_*	Re_*	θ	Pattern
...	g	g	...	...	...	kg/m^3	mm	m/s	...	...	...
0.06	10.0	10.0	61115	61115	0.00	2500	0.5	0.0159	3	0.086	Chasing
0.07	1.0	8.0	6112	48892	0.78	2500	0.5	0.0141	7	0.027	Merging
0.04	0.3	14.0	28648	1336902	0.96	2500	0.2	0.0159	3	0.086	Exchange
0.07	2.0	8.0	190986	763944	0.60	2500	0.2	0.0159	3	0.086	Frag.-chasing
0.03	1.0	8.0	95493	763944	0.78	2500	0.2	0.0141	3	0.068	Frag.-exchange

Table S2. List of the tested conditions in the off-centered configuration. σ is the offset parameter, m_i and m_t are the masses of the impacting (upstream) and target (downstream) dunes, respectively, N_i and N_t are the numbers of grains of the impacting and target dunes, respectively, ξ_N is the dimensionless particle number, ρ_s and d are the density and mean diameter of grains, respectively, u_* is the shear velocity, Re_* is the particle Reynolds number, θ is the Shields number, and *Pattern* corresponds to the collision pattern. For definitions of σ and ξ_N, please refer to Assis and Franklin, Geophys. Res. Lett., 47, e2020GL089464, 2020, https://doi.org/10.1029/2020GL089464.

σ	m_i	m_t	N_i	N_t	ξ_N	ρ_s	d	u_*	Re_*	θ	Pattern
...	g	g	...	...	...	kg/m^3	mm	m/s	...	...	...
0.60	10.0	10.0	61115	61115	0.00	2500	0.5	0.0141	7	0.027	Chasing
0.53	1.0	8.0	6112	48892	0.78	2500	0.5	0.0141	7	0.027	Merging
0.36	0.5	6.0	47746	572958	0.85	2500	0.2	0.0159	3	0.086	Exchange
0.29	6.0	8.0	572958	763944	0.14	2500	0.2	0.0159	3	0.086	Frag.-chasing
0.33	2.0	8.0	190986	763944	0.60	2500	0.2	0.0159	3	0.086	Frag.-exchange